

Dynamic Pressure Fluctuations in Stepped Three-Side Spillway

¹Hamed Taghizadeh, ²Seyed Ali Akbar Salehi Neyshabour
and Firouz Ghasemzadeh

¹Department of Hydraulic Structures, Tarbiat Modares University, P.O. Box: 14155-4838, Tehran, Iran

²Department of Civil Engineering Tarbiat Modares University, P.O. Box: 14155-4838, Tehran, Iran

³ Department of Hydraulic Structures, University of Tehran, P.O. Box: 31587-77871, Karaj, Iran

(Received: December 13, 2011; Accepted: January 12, 2012)

Abstract: One type of outlet works in dams are Three-side spillways that despite of their hydraulic limitations and construction problems, they were being selected, in storage dams, as best option under specific topographical conditions. Considerable energy losses and great turbulence are hydraulic characteristic of these spillways. Hydraulic performance with targeting to reduce pressure fluctuations in side channel is an important issue in this type of spillways design. In this study, effect of stepping of three-side spillway's Ogee profile on the dynamic pressure fluctuation have been investigated using finite volume method and RNG turbulence model. The turbulence intensity as a dimensionless number was used for quantitative study of dynamic pressure fluctuations. The results showed that the proposed form of ogee profile caused a significant reduction in turbulence intensity within the side channel. On the other hand, the stepped Ogee profiles of three-side spillways caused to simple construction and ease of operation.

Key words: Three-side spillway % Stepped Spillway % Dynamic pressure fluctuation % RNG turbulent model

INTRODUCTION

Side channel spillways are widely used in dam outlet works to irrigation and drainage networks and also used water and wastewater facilities. A special type of these spillways is the Three-sided channel spillway in which the flow enters the side channel through both the end and sides of the spillway [1]. There is a variety of names for these spillways, including bathtub spillways, U-shaped spillways and duckbill spillways [2]. They are used in situations where a spillway with a long crest is required. In Three-side spillways, the flow enters through a U-shaped weir (in plan) into the side channel that serves to deliver water downstream (Fig. 1). The flow in the side channel is a spatially varied flow with increasing discharge and is especially designed with a nonprismatic cross section (increasing bed width along the flow direction) to avoid channel flow effects on influent flows.

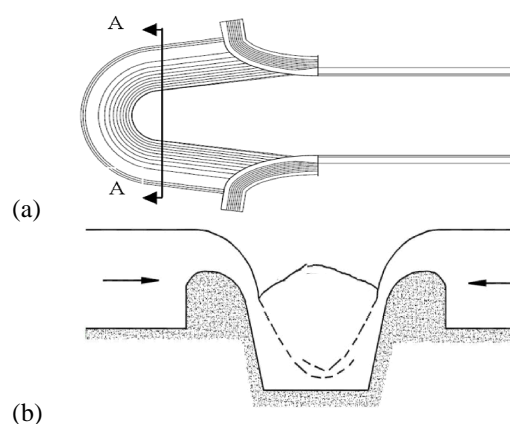


Fig. 1: Schematic views of a Three-side spillway: (a) plan view (b) section A-A

Several studies have been carried out to gain a clearer understanding of the factors affecting and the relations dominating the flow in one-sided channels. Included in these studies are the works of Bremen and

Hager [3], Farney and Markus [4], Hinds [5], Kouchakzadeh and Vatankhah [6], Kouchakzadeh *et al.* [7] and Yen and Wenzel [8]. Few studies have been done on the hydraulic performance of Three-sided channel spillways, however, most studies have only focused on specific applications of these spillways situations and have aimed at improving the hydraulic performance of the flow. Examples include the laboratory experiments by the Water Research Center [9, 10] and Knight [11]. The studies by the Water Research Center have been carried out on hydraulic models of three dams in Iran, namely Shahid Yaaghoobi, Jareh and Sivand, basically aimed at optimizing the flow conditions in the spillways. These studies focused on determining optimized values for three design parameters: side channel bed slope, the appropriate elevation and shape of the end sill for the spillways. Knight calculated the effective crest length for two-sided, L-shaped spillways, taking into account the effect of each of the corners of the spillway on reducing crest length. He also compared the curves of flow rate versus water depth above the spillway crest as obtained from theoretical and experimental methods [9, 10, 11].

A series of experimental studies on number of Three-side spillways parameters, affecting the hydraulic performance, have been carried out by Montazar and Salehi [11]. For more detailed studies, they have been defined the pressure fluctuations as an objective function.

The main findings of these laboratory researches can be summarized in the following paragraphs:

- C Turbulence intensity and pressure fluctuations in the central axis of the three-sided channel are lower than those in other parts of the channel.
- C The most important factor involved in reducing turbulence intensity and improving the hydraulic conditions in the side channel of three-sided spillways is increased flow depth inside the channel.
- C An increase in inflow rate is associated with a corresponding reduction in pressure fluctuations in the side channel and thus the flow becomes more stable.
- C Sill elevation is regarded as the most effective geometric variable for reducing turbulence intensity and pressure fluctuations in these spillways and adjusting sill elevation leads to the desired performance of the structure. Extremely high elevations, however, cause the spillway inflow to be submerged and reduce the discharge coefficient. On the other hand, extremely low sill elevations will not have any considerable effect on optimizations of the hydraulic behavior of the flow in the side channel.

- C The location of the end sill does not have a great effect on turbulence intensity. It is recommended that no sill be installed at the end section of the channel because this might give rise to interactions between the flow on the sill and the bulging flow within the central zone of the channel and thus undesirable hydraulic conditions might be created in the channel flow. To avoid this problem, it would be appropriate to install a sill close to the downstream section of the end of the side channel.
- C If possible, the side channel bed slope should be negative and about -2% to -3%. This might, of course, result in problems with construction and high costs. If a negative bed slope is adopted, however, certain provisions should be made for the drainage of the channel when the spillway is not operating. In most cases, positive channel bed slopes are selected as a desirable option. Under these conditions, a bed slope of 2%-3% is recommended [12].

Of the changes that can be utilized in three-side spillways, with a view to improving hydraulic performance, is stepping the ogee profile of spillway. The main hydraulic advantage of stepped spillways (Fig. 2) is the ability to dissipate more energy than conventional smooth spillways. Although this is a strong reason to use stepped spillways, it was not until the improvement of roller compacted concrete (RCC) technology by the end of the twentieth century that the interest in stepped spillways was definitively renewed. Currently, there is a considerable interest in evaluating the performance of stepped spillways over RCC dams for high specific discharges, in either the design of new spillways, or the re-analysis of existing spillways due to an update in the probable maximum flood. In general terms, for moderate unit discharges, large quantities of air entrain upstream of the spillway toe after the boundary layer reaches the water depth. For higher specific discharges, the boundary layer cannot reach the free surface at relatively short distances and the non-aerated region dominates large portions of the flow in the spillway.

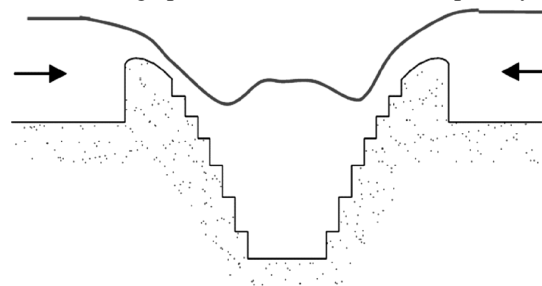


Fig. 2: Sectional view of a stepped Three-side spillway

The only disadvantage with stepped spillway is that at large discharges, as the jet is not aerated for some distance downstream of the spillway, low pressure may occur and lead to cavitations damage [1, 2].

Stepping the standard profiles of Three-side spillways has consequences such as high energy dissipation, reducing the input flow velocity around the side channel and intensity of layer abscission of approach flow within the side channel and subsequently has been caused to decrease the turbulence intensity in the side channels bed [1, 2].

In this research, the dynamic pressure fluctuation has been investigated by a commercially available CFD solver; Flow-3D, created by Flow Science. The laboratory results of Jareh dam spillway related Water Research Center, has been used for numerical model validation. The numerical results have been indicated that stepped Ogee spillway caused to reduce the dynamic pressure fluctuations in the side channels bed but this type of spillway have disadvantages such as difficult to construction and operation and larger stilling basin.

Governing Equations and Computational Scheme: To solve the governing equations of fluid flow, Flow-3D solves a modification of the commonly used Reynolds-average Navier-Stokes (RANS) equations. The modifications include algorithms to track the free surface and model the flow past obstacles such as spillways. The modified RANS equations are shown as:

$$\text{Continuity: } \frac{\partial}{\partial x}(uA_x) + \frac{\partial}{\partial y}(vA_y) + \frac{\partial}{\partial z}(wA_z) = 0 \quad (1)$$

$$\text{Momentum: } \frac{\partial U_i}{\partial t} + \frac{1}{V_F} \left(U_j A_j \frac{\partial U_i}{\partial x_j} \right) = \frac{1}{\rho} \frac{\partial P'}{\partial x_i} + g_i + f_i \quad (2)$$

The variables u , v and w represent the velocities in the x -, y - and z -directions; V_F = volume fraction of fluid in each cell; A_x , A_y and A_z = fractional areas open to flow in the subscript directions; subscripts i and j represent flow directions; D = density; P' is defined as the pressure; U_j and A_j are velocity and cell face area in the subscript direction, respectively; g_i = gravitational force in the subscript direction; and f_i represents the Reynolds stresses for which a turbulence model is required for closure. It can be seen that, in cells completely full of fluid, V_F and A_j equal 1, thereby reducing the equations to the basic incompressible RANS equations [13].

Turbulences Model: More recent turbulence models are based on Renormalization-Group (RNG) methods. This approach applies statistical methods for a derivation of the averaged equations for turbulence quantities, such as turbulent kinetic energy and its dissipation rate. The RNG-based models rely less on empirical constants while setting a framework for the derivation of a range of models at different scales. The RNG model uses equations similar to the equations for the k - ϵ model. However, equation constants that are found empirically in the standard k - ϵ model are derived explicitly in the RNG model. The transport equation for k is [14]:

$$\frac{\partial k}{\partial t} + u \frac{\partial k}{\partial x} + v \frac{\partial k}{\partial y} + w \frac{\partial k}{\partial z} = P + G + D_k - \epsilon \quad (3)$$

Where k is the turbulent kinetic energy, ϵ is the turbulent dissipation, u , v and w are velocities in x , y and z directions, respectively. P is the turbulence production term and in Cartesian coordinates is:

$$P = \frac{C_{SP} \rho}{\rho} \left[2 \left(\frac{\partial u}{\partial x} \right)^2 + 2 \left(\frac{\partial v}{\partial y} \right)^2 + 2 \left(\frac{\partial w}{\partial z} \right)^2 + \left(\frac{\partial v}{\partial x} + \frac{\partial u}{\partial y} \right)^2 + \left(\frac{\partial u}{\partial z} + \frac{\partial w}{\partial x} \right)^2 + \left(\frac{\partial v}{\partial z} + \frac{\partial w}{\partial y} \right)^2 \right] \quad (4)$$

Where D is fluid density, μ is dynamic viscosity; C_{SP} is the shear production coefficient. In Eq. (3), G is the buoyancy production term:

$$G = \frac{C_{\rho} \rho}{\rho^3} \left[\frac{\partial \rho}{\partial x} \frac{\partial p}{\partial x} + \frac{\partial \rho}{\partial y} \frac{\partial p}{\partial y} + \frac{\partial \rho}{\partial z} \frac{\partial p}{\partial z} \right] \quad (5)$$

Where C_{ρ} has a default value of 0.0, unless the problem is thermally buoyant, in which case it takes on the value of 2.5. The diffusion term, D_k in Eq. (3) is:

$$D_k = \frac{\partial}{\partial x} \left(\nu_T \frac{\partial k}{\partial x} \right) + \frac{\partial}{\partial y} \left(\nu_T \frac{\partial k}{\partial y} \right) + \frac{\partial}{\partial z} \left(\nu_T \frac{\partial k}{\partial z} \right) \quad (6)$$

Where ν_T is turbulent viscosity $F_k = 1.0$ in the standard k - ϵ model and $F_k = 0.72$ in the RNG k - ϵ model.

The transport equation for ϵ is

$$\frac{\partial \epsilon}{\partial t} + u \frac{\partial \epsilon}{\partial x} + v \frac{\partial \epsilon}{\partial y} + w \frac{\partial \epsilon}{\partial z} = C_{\epsilon 1} \frac{\epsilon}{k} (P + C_{\epsilon 3} G) + D_{\epsilon} - C_{\epsilon 2} \frac{\epsilon^2}{k} \quad (7)$$

Where C_{g1} , C_{g2} and C_{g3} are user-adjustable, non-dimensional parameters. The default value for C_{g1} is 1.44 for the $\text{RNG-k-}\epsilon$ model and 1.42 for the RNG. C_{g2} defaults to 1.92 for the $\text{RNG-k-}\epsilon$ and is computed based on the values of $\text{RNG-k-}\epsilon$ and the shear rate for the RNG model. C_{g3} has a value of 0.2 for both models. The diffusion term for the dissipation is:

$$D_e = \frac{\partial}{\partial x} \left(\frac{\nu_T}{s_e} \frac{\partial e}{\partial x} \right) + \frac{\partial}{\partial y} \left(\frac{\nu_T}{s_e} \frac{\partial e}{\partial y} \right) + \frac{\partial}{\partial z} \left(\frac{\nu_T}{s_e} \frac{\partial e}{\partial z} \right) \quad (8)$$

Where $F_g = 1.3$ in the standard $\text{RNG-k-}\epsilon$ model and $F_g = 0.72$ in the RNG $\text{RNG-k-}\epsilon$ model.

Generally, the RNG model has wider applicability than the standard k- ϵ model. In particular, the RNG model is known to describe more accurately low intensity turbulence flows and flows having strong shear regions [15].

For simple flows, where the turbulence is in local equilibrium, the model provides results similar to the standard model. For unbalanced current, especially when secondary currents are in flow, RNG model with revised coefficients provides low diffusion than the standard model. In other words, can express that the predicted viscosity values will not be increased unusually and this is considered an advantage [16].

Numerical Methodology: The commercially available CFD package Flow-3D uses the finite-volume method to solve the RANS equations [17]. The computational domain is subdivided using Cartesian coordinates into a grid of variable-sized hexahedral cells. For each cell, average values for the flow parameters (pressure and velocity) are computed at discrete times using a staggered grid technique. The staggered grid places all dependent variables at the center of each cell with the exception of the velocities u , v and w and the fractional areas A_x , A_y and A_z . Velocities and fractional areas are located at the center of cell faces (not cell centers) normal to their associated direction. For example, u and A_x are located at the center of the cell faces that are located in the Y, Z plane (normal to the X -axis). A two-equation renormalized group theory model was used for turbulence closure [13].

The modeling of a free-surface flow over an obstacle with Flow-3D constrains the makeup of each cell within the grid to one of five conditions: completely solid, part solid and fluid, completely fluid, part fluid and completely empty. The ogee crested spillway was defined as an obstacle in the rectangular domain by the implementation of the Fractional Area/Volume Obstacle Representation (FAVOR) method. The free surface was computed using a modified volume-of-fluid (VOF) method [17].

Obstacle Generation: The FAVOR method, outlined by Hirt and Nichols [18], is a porosity technique used to define obstacles. The grid porosity value is zero within obstacles and 1 for cells without the obstacle. Cells only partially filled with an obstacle have a value between zero and 1, based on the percent volume that is solid. Therefore, the ogee crest's surface is defined by cells within the grid that have a porosity value between 1 and zero. The location of the interface in each cell is defined as a first-order approximation. A straight line in two dimensions and a plane in three dimensions, determined by the points where the obstacle intersects the cell faces. The slicing plane not only defines the fractional volume that can contain fluid but also determines the fraction area (A_x , A_y and A_z) on each cell face through which flux (fluid flow) can occur. This method eliminates the "stair-stepping" effect normally associated with rectangular grids and replaces all obstacle surfaces, curved or otherwise, with short, straight-lined segments. In essence, the ogee crest is constructed of a series of short chords that define the ogee's curves. Given this fact, it is obvious that smaller size cells produce a much smoother numerical obstacle boundary. It is important to note that, although short chords can effectively approximate a curved surface, it is still an approximation to a curved surface. To fit a curved surface exactly, a different numerical method such as a second order finite-element method or a curvilinear boundary fitted method would be required [18].

Free Surface: To numerically solve the rapidly varying flow over an ogee crest, it is important that the free surface be accurately tracked. Tracking involves three parts: locating the surface, defining the surface as a sharp interface between the fluid and air and applying boundary conditions at the interface. One means of tracking the free surface is the VOF method. The VOF method evolved from the marker-and-cell method but is more computationally efficient. The VOF method is also described by Hirt and Nichols [18]. The VOF method is similar to the FAVOR method in defining cells that are empty, full, or partially filled with fluid. Cells without fluid have a value of zero. Full cells are assigned a value of 1 and partially filled cells have a value between zero and 1. The slope of the free surface within the partial cells is found by an algorithm that uses the surrounding cells to define a surface angle and a surface location. The VOF method allows for steep fluid slopes and breaking waves. Similar to the FAVOR method, the free surface is defined by a series of connected chords (2D) or by connected planes (3D); however, the VOF method allows for a

changing free surface over time and space. Once again, this first-order approximation is not an exact fit to the curved flow surface. A true fit would require a second-order or higher adaptive grid that changes temporally and spatially to fit the changing water surface. The VOF method has additional concerns that require special consideration. VOF numerical techniques tend to be dissipative in nature, which can smear the free surface interface. Smearing of the interface distributes small amounts of fluid across several adjacent cells. These “misty” cells can introduce spurious results and prevent the free surface from being accurately identified. Flow-3D reduces this problem by implementing an algorithm to effectively clean up the misty regions [17]. The implementation of this algorithm eliminates fluid in the misty regions and resets the fluid fraction in interface cells, thereby not completely adhering to the conservation of mass principle. The conservation of mass principle is additionally violated by computer round off error, as the code tracks fluid flux through cell face areas. However, the code also tracks the volume of fluid that is eliminated or added to the solution by the different algorithms. This cumulative volume error can provide a means of monitoring and evaluating the solution accuracy. In the final run of each numerical simulation, a cumulative volume error of less than 60.03% was reported. Therefore it is believed that the effect on continuity was not significant, for all practical purposes [18, 19].

Model Validation: The laboratory results of Jareh dam’s spillway related Water Research Center has been used for numerical model verification. In order to verification, the numerical model of Jareh dam’s spillway (Fig. 3) was simulated and then the results were compared with experimental results.

Flow Pattern: The flow pattern observed in different experiments shows a bulge in the flow surface at the central zone of the spillway’s side channel (Fig. 4) that major cause of this bulge may be related to the collision of the inflows in this zone and conversion of their momentum to pressure that this pressure shows itself as a rise in depth. For lower inflow discharges, the momentum of the inflow is low too and so the pressure and flow depth within the central zone of the channel will be low. Under such circumstances, the flow depth at the peripheries of the bulge is unstable and there are large fluctuations in flow depth towards the channel sidewalls.

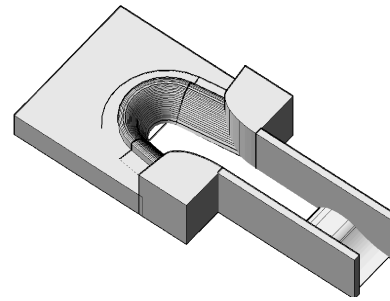


Fig. 3: Three dimensional solid of simulated model

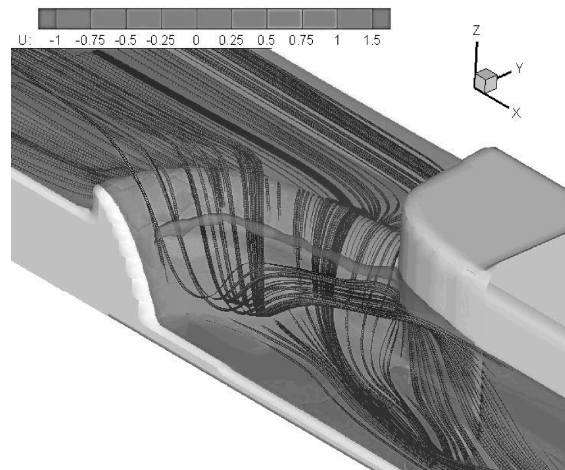


Fig. 4: Flow pattern and streamline on the spillway ($Q=55$ l/s)

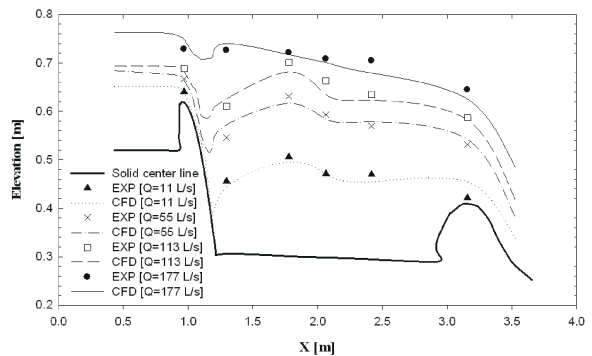


Fig. 5: Flow depth at the central axis of the side channel for different discharges. (CFD-Experimental)

Flow Depth at the Central Axis of the Side Channel: According to the available experimental data, values of flow depth at central axis of the side channel have been gained. Fig. 5 shows the numerical and experimental values of flow depth at central axis of the side channel.

This result shows that the model is so capable in determination of the water surface profiles in the side channel. The flow patterns observed from different experiments shows formation of a bulge in the flow depth

Table 1: Information about meshing, boundary conditions and equations

Meshing	Model Type	VOF
	Number of computational blocks	2
	Number of computational Volume	500000
Boundary conditions	Spillway body	Solid
	Lateral boundaries	Wall
	Inlet	Specific Velocity
Equations	Outlet	Outlet
	Turbulence model	RNG
	Algorithm to solve the pressure equation	GMRES
	Algorithm to solve the fluid shear stress	Explicit
	Free surface model	VOF
	Time interval	0.01s

Table 2: Cross sectional flow depths (cm) for different discharges

a. Q=11 l/s							
Type	Experimental			CFD			Error %
Sections	Right	Center	Left	Right	Center	Left	
B	15.0	14.5	15.0	14.3	14.00	14.4	3.40
C	17.0	20.5	16.8	18.0	19.45	17.6	5.12
D	18.1	17.3	18.0	17.8	17.26	17.6	0.23
E	19.3	18.6	19.0	18.8	17.80	18.5	3.90
b. Q=55 l/s							
Type	Experimental			CFD			Error %
Sections	Right	Center	Left	Right	Center	Left	
B	23.4	23.0	23.5	21.0	22.45	22.3	2.40
C	26.0	33.0	26.5	26.7	32.20	26.3	2.42
D	28.1	29.5	28.5	28.1	28.51	27.4	3.30
E	27.5	27.5	27.5	27.4	28.55	27.7	3.80
c. Q=113 l/s							
Type	Experimental			CFD			Error %
Sections	Right	Center	Left	Right	Center	Left	
B	30.8	30.5	30.7	30.5	30.2	30.5	1.0
C	33.0	39.6	32.8	32.1	37.9	31.0	4.2
D	33.4	36.5	33.5	32.5	35.0	32.7	4.1
E	34.7	34.5	34.8	33.4	33.2	33.3	3.7
d. Q=177 l/s							
Type	Experimental			CFD			Error %
Sections	Right	Center	Left	Right	Center	Left	
B	41.6	42.0	42.0	43.0	43.0	42.8	2.3
C	42.4	42.2	42.6	42.0	42.0	42.2	0.5
D	40.9	41.7	40.8	40.0	41.1	41.0	1.4
E	41.2	41.0	41.2	39.7	39.7	40.0	3.1

at central zone of the spillway's side channel. It may be resulted from collision of the inflows in this zone. When the inflows, perpendicular to the axial flow, collide at the side channel, the momentum of them cause to rise in pressure and this pressure manifests itself as an increase in flow depth at central zone. For lower inflow discharges, the momentum of the inflow into the side channel is correspondingly low so the pressure and flow depth

within the central zone of the channel will be comparatively low. Under such circumstances, the flow depth at the peripheries of the bulge is also lower and the bulge does not have great stability, so there are large fluctuations in flow depth towards the channel sidewalls. For this reason, in the bulge station, calculations in terms of location are with large errors. By considering that the most important factor involved in reducing turbulence

intensity and improving the hydraulic conditions of three-sided spillway's side channel is increased flow depth of channel, a significant error is occurred at the less discharges.

The Cross Sectional Flow Depth: Considering that the flow is three-dimensional, the cross sectional flow depth has been gained in sections B, C, D and E (Fig. 6). Table 2 shows the numerical and experimental values of the cross sectional flow depth that are calculated in the specified sections of Fig. 6. In addition, Fig. 7 shows that how the bulge comes up.

Analysis of Dynamic Pressure Fluctuations: In this study, in order to quantitative analyze of the dynamic pressure fluctuations, a dimensionless number called the turbulence intensity has been used and can be calculated from the following relations [12]:

$$T_u = \frac{P'_{rms}}{\bar{P}} \quad (9)$$

Where

$$\bar{P} = \lim_{T \rightarrow \infty} \frac{1}{T} \int^T P(t) dt \quad (10)$$

and

$$P'_{rms} = \sqrt{P'^2} = \lim_{T \rightarrow \infty} \left[\frac{1}{T} \int^T P'(t)^2 dt \right] \quad (11)$$

In which P'_{rms} is the root mean square of the momentary pressure, \bar{P} is the average pressure, P' is the instantaneous pressure, T is the time cycle of the pressure fluctuation, t is the time parameter.

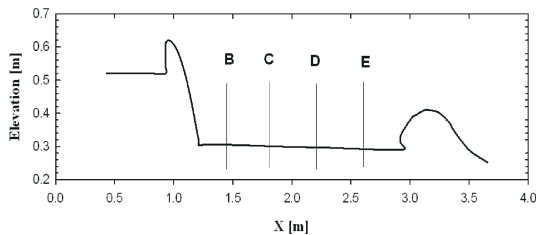


Fig. 6: Location of cross sections for study of flow properties

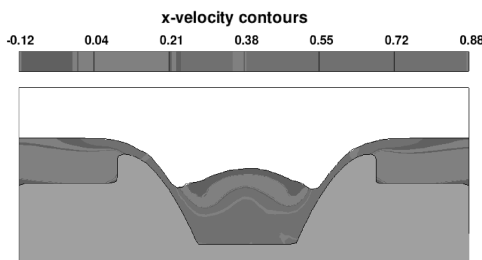


Fig. 7: Bulge's come up in C section (Q=55 l/s)

RESULTS AND DISCUSSION

Dynamic Pressure Fluctuations: For investigation of dynamic pressure fluctuations, a series of important points in side channel spillway (Fig. 8) were chosen, then the Instantaneous pressure and turbulence parameters were calculated.

Table 3: Turbulence intensity parameter values in main points of the sill (Figure 8) in the side channel

T_u			T_u		
Q=113 l/s			Q=11 l/s		
Point	Ogee	Stepped	Point	Ogee	Stepped
1	0.00134	0.00372	1	0.35347	0.18122
2	0.02380	0.00060	2	0.01769	0.02124
3	0.02303	0.00063	3	0.00925	0.01223
4	0.02303	0.00063	4	0.00925	0.00223
5	0.02271	0.00071	5	0.01453	0.00958
6	0.02205	0.00077	6	0.02934	0.03393
7	0.02205	0.00077	7	0.02934	0.03393
8	0.02014	0.00083	8	0.01459	0.00712
9	0.01954	0.00064	9	0.01631	0.00885
10	0.01954	0.00064	10	0.01631	0.00885
11	0.01443	0.00070	11	0.00320	0.00159
12	0.01408	0.00090	12	0.02177	0.04945
13	0.01408	0.00090	13	0.02177	0.01945
14	0.00588	0.00051	14	0.00280	0.00191
15	0.00621	0.00058	15	0.00253	0.00187
16	0.00621	0.00058	16	0.00253	0.00187

T_u			T_u		
Q=177 l/s			Q=55 l/s		
Point	Ogee	Stepped	Point	Ogee	Stepped
1	0.00232	0.00637	1	0.01270	0.01973
2	0.00137	0.00049	2	0.01447	0.00556
3	0.00130	0.00049	3	0.02046	0.00778
4	0.00130	0.00049	4	0.02046	0.00778
5	0.00123	0.00052	5	0.01088	0.00636
6	0.00119	0.00050	6	0.01099	0.00386
7	0.00119	0.00050	7	0.01099	0.00386
8	0.00093	0.00053	8	0.00907	0.00316
9	0.00089	0.00054	9	0.00870	0.00458
10	0.00089	0.00054	10	0.00870	0.00458
11	0.00062	0.00064	11	0.00756	0.00188
12	0.00058	0.00066	12	0.02186	0.00216
13	0.00058	0.00066	13	0.02186	0.00216
14	0.00055	0.00060	14	0.00476	0.00126
15	0.00057	0.00064	15	0.00472	0.00159
16	0.00057	0.00064	16	0.00472	0.00159

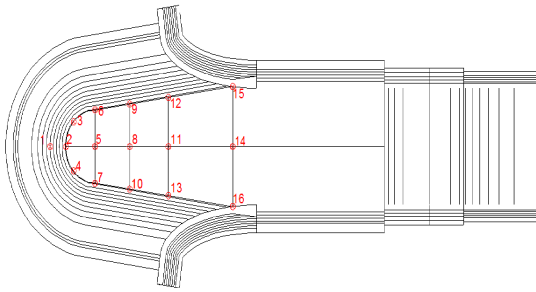


Fig. 8: Distribution of the selected set of main point of the sill in the model

As regards the most important factor involved in reduction of turbulence intensity and improving the hydraulic conditions in the side channel of three-sided spillways is increased flow depth inside the channel, flow depth in the Central axis of side channel was extracted. Instantaneous pressure at 5 second period was taken and turbulence intensity was calculated after a series of mathematical operations. For example, at point 8 pressure fluctuations has been shown in Fig. 9.

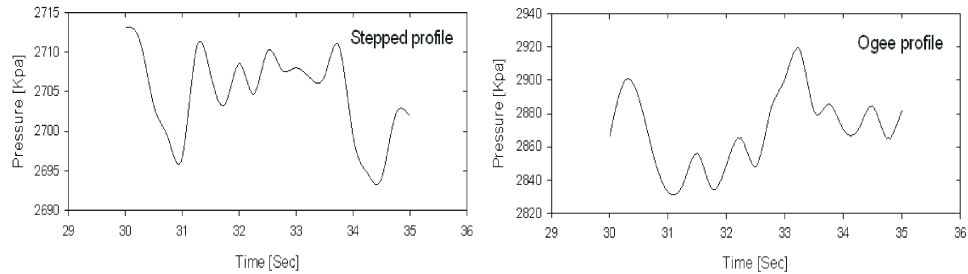


Fig. 9: Pressure fluctuation at point 8 ($Q=55$ l/s)

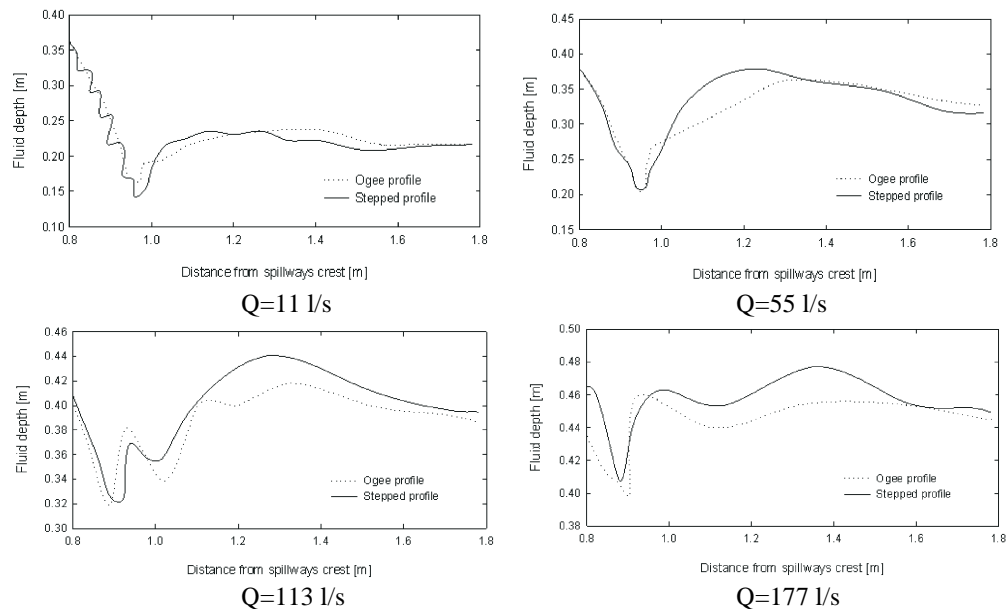


Fig. 10: Flow depth at central axis of the side channel for different discharges

The quantity of turbulence intensity in main point has been presented in Table 3. According to these tables, the pressure is increased and flow condition is improved due to increasing the input discharge.

As it moves downstream of the channel, amount of turbulence and flow Collision decrease so the turbulence intensity decreases. Results are shown the high turbulence intensities in the beginning and in the edges of side channel.

The most important effect of stepped ogee profile of Three-side spillway is increase in energy dissipation and decreasing the flow Collision. During of decrease in flow Collision, as has been shown in Fig. 10, a significant increase in the flow depth in the side channel will not seen, but due to a delay in discharging the flow from side channel, flow depth increased slightly and the increasing of flow depth is more noticeable on the edge of the channel. This will help to reduce pressure fluctuations in side channel, but the most important factor that involve in reducing the turbulence intensity is decrease of flow turbulence due to decrease in flow collision.

This results shows that the effect of stepping has been decreased by increasing of discharge.

CONCLUSION

In this study, by using the numerical modeling and with emphasis on the stepped spillway, amount of dynamic pressure fluctuations was investigated and the following results were obtained:

- C The features and benefits that can be allocated for typical stepped spillways could be said for the Three-side stepped spillways. Stepping the ogee profile of Three-side spillway will cause the reduction on the velocity and flow energy with creation of roughness. In addition, will cause the increasing of self-purification of river due to good aeration.
- C The possibility of negative pressure event and cavitations on spillway has been reduced by stepping of the ogee profile of Three-side spillway.
- C In general can be said that the amount of dynamic pressure fluctuation in the side channel bed has been decreased considerably by stepping the ogee profile of Three-side spillway.
- C The dynamic pressure fluctuations reduction, most occurred in areas of side channel where the minimal effect of flow collides involves.
- C In stepped Three-side spillway, the dynamic pressure fluctuations during the side channel reduce quickly.
- C Flow depth in the Side channel of stepped Three-side spillway is more than the standard crest and this fact plays an important role in reducing of the turbulence intensity.
- C Stepping of the Ogee profile of Three-side spillway, apart from the hydraulic advantages, causes the ease of construction and operation of this kind of spillways.

Nomenclature:

D	Dissipation Function
D	Fluid density
σ	Surface tension coefficient
T_u	Turbulence intensity
P'_{rms}	Root mean square of instantaneous pressure fluctuations
T	Cycle of pressure changes
\bar{P}	Pressure average
f_i	Reynolds stresses

u, v and w	Velocities in the x -, y - and z -directions
V_F	Volume fraction of fluid in each cell
A_x, A_y and A_z	Fractional areas open to flow in the subscript directions
P'	pressure
g_i	gravitational force in the subscript direction
k	Turbulent kinetic energy
ϵ	Turbulent dissipation
P	Turbulence production term
μ	Dynamic viscosity
C_{SP}	Shear production coefficient
G	Buoyancy production term
D_k	Diffusion term
ν_T	Turbulent viscosity

REFERENCES

1. Bremen, R. and W.H. Hager, 1989. Experiments in side channel spillways. ASCE J. Hydraulic Engineering, 115(5): 617-635.
2. Farney, H.S. and A. Markus, 1962. Side channel spillway design. ASCE J. the Hydraulics Division, 88(3): 131-154.
3. Hinds, J., 1926. Side channel spillway. Transactions of the American Society of Civil Engineers, 89: 881-927.
4. Kouchakzadeh, S. and A.R. Vatankhah Mohammad-Abadi, 2002. Spatially varied flow in non-prismatic channels: dynamic equation. Irrigation and Drainage (J. the International Commission on Irrigation and Drainage), 51(1): 41-50.
5. Kouchakzadeh, S., M.K. Kholghi and A.R. Vatankhah Mohammad-Abadi, 2002. Spatially varied flow in non-prismatic channels: numerical solution and experiment verification. Irrigation and Drainage (J. the International Commission on Irrigation and Drainage), 51(1): 51-60.
6. Yen, B.C. and H.G. Jr. Wenzel, 1970. Dynamic equations for steady varied flow. ASCE J. the Hydraulics Division, 96(3): 801-814.
7. Water Research Center, 1994. Final report of hydraulic model of Shahid Yaaghoobi. Ministry of Energy of Iran, Iran. Report 161. [In Farsi.].
8. Water Research Center, 1996. Final report of hydraulic model of Jareh. Ministry of Energy of Iran, Iran. Report 268. [In Farsi.].
9. Knight, A., 1989. Design of efficient side channel spillway. ASCE J. Hydraulic Engineering, 115(9): 1275-1289.

10. Montazar, A. and S.A.A. Salehi Neyshabouri, 2006. Impact of Some Parameters Affecting the Hydraulic Performance of U-shaped Side Spillway. *Canadian J. Civil Engineering*, 33: 552-560.
11. Jansen, I. and B. Robert, 1988. *Advanced dam engineering for design, construction and rehabilitation*. Van Nostrand Reinhold, New York.
12. US Bureau of Reclamation, 1974. *Design of small dams*. 2nd ed. US Government Printing Office, Washington, D.C.
13. Ferziger, J. and M. Peric, 1996. *Computational methods for fluid dynamics*. Springer Verlag.
14. Isfahani, A.H.G. and J.M. Brethour, 2009. On the Implementation of Two-equation Turbulence Models in FLOW-3D, Flow Science, Inc., FSI-09-TN86.
15. Bradshaw, P., 1996. The Understanding and Prediction of Turbulent Flow. *International J. Heat and Fluid Flow*.
16. Bradshaw, P., 1987. Turbulent Secondary Flows. *Annual Review of Fluid Mechanic*, pp: 53-74.
17. http://www.flow3d.com/resources/tech_paper/res_tp_main.html.
18. Hirt, C. and B. Nichols, 1981. Volume of Fluid (VOF) Method for the Dynamics of Free Boundaries.
19. Kim, D. and H. Choi, 2000. A second-order time-accurate finite volume method for unsteady incompressible flow with hybrid unstructured grids. *J. Computational Physics*, 162: 411-428.